remote sensing

MDPI

Article

Long-Term Post-Disturbance Forest Recovery in the Greater Yellowstone Ecosystem Analyzed Using Landsat Time Series Stack

Feng R. Zhao [1,*], Ran Meng [2], Chengquan Huang [1], Maosheng Zhao [1], Feng A. Zhao [1], Peng Gong [3], Le Yu [3] and Zhiliang Zhu [4]

1 Department of Geographical Sciences, University of Maryland, College Park, MD 20742, USA; cqhuang@umd.edu (C.H.); zhaoms@umd.edu (M.Z.); zhao26@umd.edu (F.A.Z.)
2 Environmental and Climate Sciences Department, Brookhaven National Laboratory, Bldg. 490A, Upton, NY 11973, USA; ranmeng@bnl.gov
3 Ministry of Education Key Laboratory for Earth System Modeling, Center for Earth System Science, Tsinghua University, Haidian, Beijing 10083, China; penggong@tsinghua.edu.cn (P.G.); leyu@tsinghua.edu.cn (L.Y.)
4 U.S. Geological Survey, Reston, VA 20192, USA; zzhu@usgs.gov
* Correspondence: fengzhao@umd.edu; Tel.: +1-240-485-6468

Academic Editors: Angela Lausch, Marco Heurich, Josef Kellndorfer and Prasad S. Thenkabail
Received: 20 April 2016; Accepted: 21 October 2016; Published: 29 October 2016

Abstract: Forest recovery from past disturbance is an integral process of ecosystem carbon cycles, and remote sensing provides an effective tool for tracking forest disturbance and recovery over large areas. Although the disturbance products (tracking the conversion from forest to non-forest type) derived using the Landsat Time Series Stack-Vegetation Change Tracker (LTSS-VCT) algorithm have been validated extensively for mapping forest disturbances across the United States, the ability of this approach to characterize long-term post-disturbance recovery (the conversion from non-forest to forest) has yet to be assessed. In this study, the LTSS-VCT approach was applied to examine long-term (up to 24 years) post-disturbance forest spectral recovery following stand-clearing disturbances (fire and harvests) in the Greater Yellowstone Ecosystem (GYE). Using high spatial resolution images from Google Earth, we validated the detectable forest recovery status mapped by VCT by year 2011. Validation results show that the VCT was able to map long-term post-disturbance forest recovery with overall accuracy of ~80% for different disturbance types and forest types in the GYE. Harvested areas in the GYE have higher percentages of forest recovery than burned areas by year 2011, and National Forests land generally has higher recovery rates compared with National Parks. The results also indicate that forest recovery is highly related with forest type, elevation and environmental variables such as soil type. Findings from this study can provide valuable insights for ecosystem modeling that aim to predict future carbon dynamics by integrating fine scale forest recovery conditions in GYE, in the face of climate change. With the availability of the VCT product nationwide, this approach can also be applied to examine long-term post-disturbance forest recovery in other study regions across the U.S.

Keywords: wildland fires; timber harvest; detectable forest recovery; 1988 Yellowstone Fires

1. Introduction

Forests in the Greater Yellowstone Ecosystem (GYE) experience frequent natural (e.g., wildfires, insect and disease outbreaks, and snow and wind damage) and anthropogenic (e.g., land use changes and timber harvesting) disturbance events [1,2]. Recovery from past disturbance is an integral process of carbon cycles [3,4]. Inclusion of the forest recovery process following disturbance is

thus critical to calculating regional carbon fluxes and can better inform policy makers on both the importance and uncertainty of disturbances in the regulation of the regional and global carbon cycles [5]. Many ecosystem models assume post-disturbance forest recovery occurs immediately or homogenously across the landscape. This modeling hypothesis, however, has not been supported by ground observations [6]. Therefore, there is an urgent need to efficiently examine forest recovery conditions at large scales.

Despite the urgent needs in quantifying post-disturbance forest recovery, a universal definition of forest recovery is not available [7]. Terminologies such as "regeneration", "regrowth", and "recovery" are often used, sometimes interchangeably, to represent the return of vegetation (including grass, shrub, and forests) following disturbances [7–9]. In the context of forest recovery, it is necessary to clearly define forest, and the recovery of forest. In this study, we defined forest following the definition of the Food and Agriculture Organization (FAO) of the United Nations, i.e., greater than 10% tree cover (FAO 1998). Forest recovery was then defined as the return of forest cover to more than 10% of the area.

This definition of forest has allowed remote sensing as a tool for examining forest disturbance and recovery over large areas [10–14], especially for fires [15–18] and logging [19–22]. Many remote sensing-based studies have made contributions to our understanding of vegetation spectral recovery following disturbances [8,23]. In particular, a series of Landsat mission satellites have been imaging the Earth's surface since 1972, creating a time series of Landsat observations that is highly valuable for tracking land change history for over four decades [24–26]. Although numerous change detection procedures have been developed [27–32], with some having succeeded in mapping forest disturbances and disturbance types over large areas [31,33–40], characterizing long-term forest spectral recovery following specific disturbance types remains challenging. Depending on local environmental conditions and post-disturbance management practices, it often takes years to decades for forests to recover its functions, following a stand-clearing disturbance event [41,42]. It is valuable to determine at what point in time during this process young trees have started to grow back and restore forest ecosystem services.

One of the algorithms, the Vegetation Change Tracker (VCT), was designed to both detect forest disturbance and track post-disturbance spectral recovery [43] using annual or biannual Landsat time series stacks (LTSSs) [44]. Although the disturbance products (tracking the conversion from forest to non-forest type) derived using this LTSS-VCT approach have been validated extensively for mapping forest disturbances across the United States [45–48], the ability of this approach to characterize post-disturbance spectral recovery has yet to be assessed. Based on the FAO forest definition, we can approximate the recovery of forest cover to more than 10% of the area with spectral values within pre-determined thresholds. Notably, a spectral recovery is not synonymous with ecological definitions of forest recovery [43]. Spectral recovery signal is also highly dependent on the choice of remote sensing index and the recovery definition. In addition, recovery does not imply that the pixel is occupied by the original species. In the GYE, for example, a post-fire Whitebark Pine forest might grow back as birch forest in the first few decades after the fire [49].

In the GYE, forest recovery trends vary from one forest type to another. This mainly has to do with species-specific regrowth attributes. Lodgepole Pine (*Pinus contorta*) and Aspen (*Populus tremuloides*) are fast-growing species that usually occupy lower elevations and may grow back in 5–20 years after a stand-clearing disturbance [50,51]. Forests that grow at higher elevations, such as Whitebark Pine (*Pinus albicaulis*), Engelmann Spruce (*Picea engelmannii*) and Subalpine Fir (*Abies lasiocarpa*), usually take longer time to recover [50]. Forest recovery trends in the GYE also differ between various land ownership and disturbance types. The post-harvest forest recovery in national forest land is generally faster than the post-fire forest recovery in both national parks and national forests, likely due to the following reasons. (1) Land productivity in national forests is generally higher than that of the national parks and wilderness areas [52]. Most fires occur at high-elevation low-productivity sites with shorter growing seasons, whereas harvested sites generally have longer growing seasons and higher site productivity; (2) Post-harvest forest management activities helped increase forest recovery rates in the

national forests. In addition to other forest management techniques used to aid forest growth, planting is a common practice in national forests, especially for harvested forests after natural regeneration fails [53]; (3) The post-disturbance forest recovery in national parks and wilderness areas is subject to threats from various wild animals, insects and diseases, and national forests usually have higher levels of protection against these factors.

The GYE has been a focal point for many post-disturbance vegetation recovery studies [9,42,54–58], yet most previous studies relied on plot-level data and were limited in their ability to densely sampling in the remote, high-elevation areas of the Yellowstone Caldera. No systematic measurement based assessment of forest recovery following disturbances has been conducted across the whole region in recent decades (1980s to the present). The specific goals of our study, as described in this paper, were as follows: (1) to validate the VCT long-term (up to 24 years) recovery product focused on tracking post-fire and post-harvest forest recovery in GYE, using year 2011 (last year of the VCT product) as a reference year for the recovery; and (2) to use the validated recovery product to analyze the recovery rates for major fires and harvests that occurred in the 1980s (to allow adequate time for recovery to occur). Results from this study shed lights to regional post-disturbance forest spectral recovery trends and bring in a time-series perspective in analyzing post-disturbance forest spectral recovery in the GYE. With the availability of VCT product nationally, this approach can be applied to other study regions in the U.S.

2. Study Area

The 91,758-km^2 study area of the GYE region includes Yellowstone National Park (YNP) and Grand Teton National Park in the center and seven surrounding national forests (Bridger-Teton, Caribou-Targhee, Gallatin, Shoshone, Custer, Helena, and Beaverhead-DeerLodge) (Figure 1).

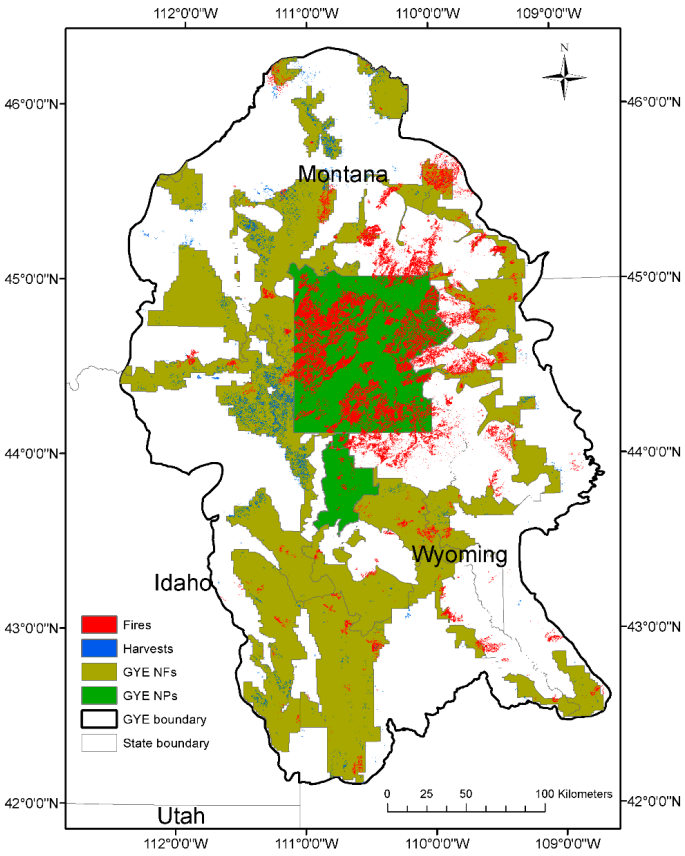

Figure 1. Boundary, ownership, and forest fires and harvests between 1985 and 2011 in the Greater Yellowstone Ecosystem (GYE). NPs stand for National Parks and NFs represent National Forests.

The GYE features distinct gradients in elevation, climate and soil. Vegetation distribution highly depends on topographical variations such as changes of elevation and aspects, and the effects of topography are manifested through its associations with temperature and moisture availability [59]. Mean annual temperature varies from 7.6 °C at lower elevations (<1400 m) to 0.13 °C at higher elevations (>2300 m) [52]. Precipitation mostly falls as snow and generally increases with elevation; mean annual precipitation ranges from 1368 mm to 2414 mm [59]. The growing season in the GYE varies from less than three months at higher elevations to around six months at lower elevations [1]. A large portion of the national parks (NPs), including the Yellowstone Plateau and surrounding mountain ranges, lies at relatively high elevations. The national forest (NF) lands are mostly at moderate and low elevations on the flanks of the plateau. The soils at higher elevations are largely composed of nutrient poor rhyolites and andesites with low water-holding capacities [59]. The valley bottoms and floodplains contain glacial outwash and alluvium soils that generally feature higher nutrients and water-holding capacities in relative terms [52].

Natural forest vegetation in the study area is a mosaic of major coniferous species [60]. Lodgepole Pine is widespread in YNP and dominates about 70% of the forested NP area (approximately 5295 out of 7355 km^2), followed by forest species such as Whitebark Pine, Subalpine Fir, Engelmann Spruce, Douglas Fir (*Pseudotsuga menziesii*) and Aspen [61]. Whitebark Pine occupies approximately 15% of the YNP forested area, especially at the higher elevations. Engelmann Spruce and Subalpine Fir often co-exist below the elevation zone of Whitebark Pine, with Douglas-fir dominating the lowest elevations. Lodgepole Pine forests between 2000 m and 2600 m are supported by rhyolite soils, and Douglas-fir can be found up to 2300 m on andesitic soils and in relative warm conditions [1]. Above these elevations in all soil types, forests types such as Subalpine Fir, Engelmann spruce, and Whitebark pine dominate. About 70% of the GYE forested area is located in national forests (Figure 1), which contain wilderness areas designated by the Wilderness Act of 1964 (~22% of the GYE forested area) and areas managed for timber production (~47.7% of GYE forested area). National parks occupy more than a quarter of the GYE forested area and the remaining forested areas are under other ownership, such as state or private forests.

The recent history and composition of disturbance events during the study interval (1984–2011) are shown in Figure 1, which also shows the effects of ownership pattern on disturbances. In the GYE national parks and wilderness area, fire was the most dominant disturbance agent, affecting over 37% of the forested area in the GYE national parks. Active harvest event was a major human-induced disturbance type occurring in the national forests. In particular, the harvested area in the Caribou-Targhee National Forest (west to the National Park) was four times larger than the burned areas during the study period [2].

3. Materials and Methods

3.1. LTSS Assembling

LTSSs from both Landsat TM and ETM sensors were assembled for the 8 Landsat World Reference System-2 (WRS-2) path/row locations required to cover the GYE (Figure 1, Landsat scenes for the study region include p37r29, p37r30, p38r28, p38r29, p38r30, p38r31, p39r28, and p39r29). The 30-m resolution Landsat images were downloaded from the USGS Global Visualization Viewer (GloVis). The original images were first converted to surface reflectance using the Landsat Ecosystem Disturbance Adaptive Processing System (LEDAPS) algorithm [61]. Geometrically, no additional correction was performed on these images because they had already been ortho-rectified by the USGS to achieve subpixel geolocation accuracy [44,61]. A detailed description of the procedures involved in assembling LTSSs has been provided in a previous study [44].

Each LTSS contained one image per year for the years between 1984 and 2011 that had at least one clear view (cloud-free or nearly cloud-free with cloud cover less than 5%) image acquired during the leaf-on growing season (May to September). If no such image was available in certain years,

multiple partly cloudy images acquired during the leaf-on growing season of that year were used to produce a composite image [43,48]. The compositing algorithm identifies and replaces the cloud and shadow contaminated pixels and adjusts the phenological differences among the affected images [44]. The cloud and cloud shadow were identified using an automated masking algorithm [43]. Omission errors for the masking algorithm were around 1% for the cloud class, although the errors were higher for low cloud cover and semiarid environment, potentially leading to higher forest and disturbance mapping errors [62]. If no more than 1 clear-view observation was available in a year at a given pixel location, the pixel with the maximum NDVI value was selected [48,63]. If more than one clear-view observation was available, the clear-view observation that had the highest brightness temperature was selected [48,64]. Here, clear-view observations referred to those that were not contaminated by clouds or shadows and did not have other data quality problems [43].

3.2. Forest Disturbance and Recovery Mapping

The LTSSs assembled in Section 3.1 were analyzed using the VCT algorithm to map forest disturbance and recovery. The VCT uses an integrated forest z-score (IFZ) index to track forest changes at each pixel location:

$$\mathrm{IFZ} = \sqrt{\frac{\sum_{\mathrm{band3,5,7}} \left(\frac{\mathrm{bi}-\overline{\mathrm{bi}}}{\mathrm{SDi}}\right)^2}{3}}, \quad (1)$$

where bi is the spectral value of a pixel in band i, and $\overline{\mathrm{bi}}$. and SDi are the mean and standard deviation of selected standard forest samples in that band, respectively, which are identified automatically using a dark object approach [43,65]. Band 3, 5 and 7 from TM and ETM sensors are used, representing Red (wavelength 0.63–0.69 um), Shortwave Infrared (wavelength 1.55–1.75 um) and Shortwave Infrared (wavelength 2.09–2.35 um) bands, respectively. The IFZ is a non-negative, inverse indicator of forest likelihood. The closer to 0 this value is, the closer to a forest pixel this value is, and the more likely the pixel is a forest pixel. The higher this value is, the more likely this pixel is a non-forest pixel [48]. When a disturbance occurs, that pixel loses part or all of its forest cover, often resulting in a sharp increase in the IFZ value. Thus, the year of disturbance is defined as the year when the IFZ value increases sharply and exceeds the range of forest pixel thresholds (for example, year 1988 in Figure 2). The IFZ then decreases gradually if trees grow back after that disturbance event. VCT uses both IFZ and NDVI to determine whether and when recovery occurred. If the IFZ and NDVI drop below the pre-determined thresholds for two consecutive years, post-disturbance recovery is considered to have occurred, and the disturbed pixel is reclassified as having forest cover after that point (Figure 2a,b). Otherwise, no recovery detected during the years covered by the LTSS (Figure 3c). While a single set of IFZ and NDVI threshold values of 3.0 and 0.45 was adequate for most closed canopy forests [43], many low canopy cover forests in the GYE region were mapped as non-forest in an initial VCT run using the threshold value set. To mitigate this problem, we used field plot data collected by the USDA Forest Service Forest Inventory and Analysis (FIA) program as reference to determine the appropriate threshold values. Specifically, for each scene, we randomly draw a pair of IFZ-NDVI threshold values, used them in the VCT forest/non-forest classification step and then calculated the agreement between the new VCT classification and the FIA reference data set. This was repeated 20,000 times for each WRS-2 tile. The range of IFZ and NDVI thresholds was bounded between 0 and 30 for IFZ and 0 and 1 for NDVI. The pair of IFZ-NDVI threshold values that yielded the highest agreement between VCT and the FIA reference data set for a WRS-2 scene were selected as the optimal VCT threshold values for that scene (Zhao et al. in preparation). The final threshold values used in this study are provided in Table S3 in the Supplementary Materials.

The VCT produces two types of recovery products. The first indicates whether detectable recovery as defined above occurred after each disturbance mapped by VCT, or recovery/no-detectable-recovery (RNR) maps. Secondly, if there was detectable recovery following a disturbance, the number of years for the regenerating trees to become detectable as forest by VCT, defined as years-until-detectable-recovery in this study (Figure 2a,b), is recorded as the second product type. Detailed descriptions of the VCT

algorithm and its disturbance products were provided in previous publications [43,46,47]. The VCT mapped harvests and fire disturbance maps were validated using the TimeSync tool by examining 400 stratified randomly sampled points in the GYE. The Overall Accuracies for the mapped fires and harvests were about 87%, with user's and producer's accuracies in the ranges 91%–96% and 73%–89%, respectively [2].

The disturbances mapped by the VCT were classified into fire, harvest, and other disturbances using a support vector machine (SVM) that has been described in a previous study [2]. We only examined areas that were disturbed once in the time interval to avoid influences from consecutive disturbances, which is a special case itself. The fire disturbances were further divided into low-, medium-, and high-severity fires using the Relative difference Normalized Burn Ratio (RdNBR). RdNBR is a remote sensing index developed for characterizing the spatial complexity of fire severity in the US [66].

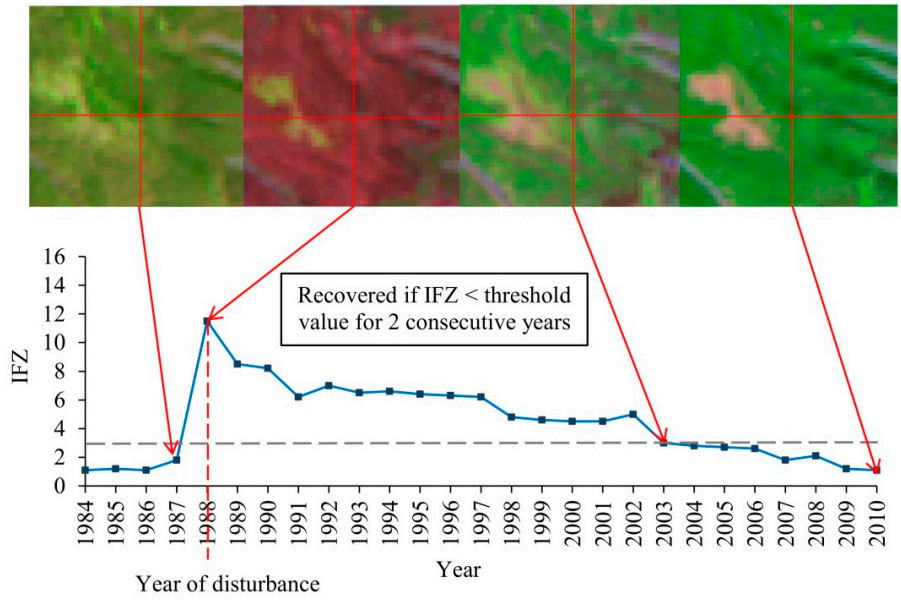

(**a**)

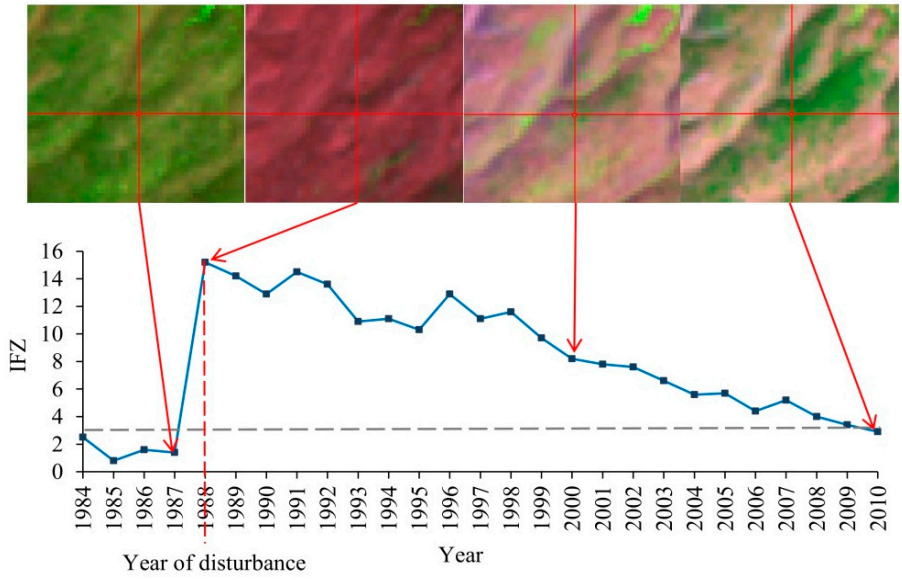

(**b**)

Figure 2. *Cont.*

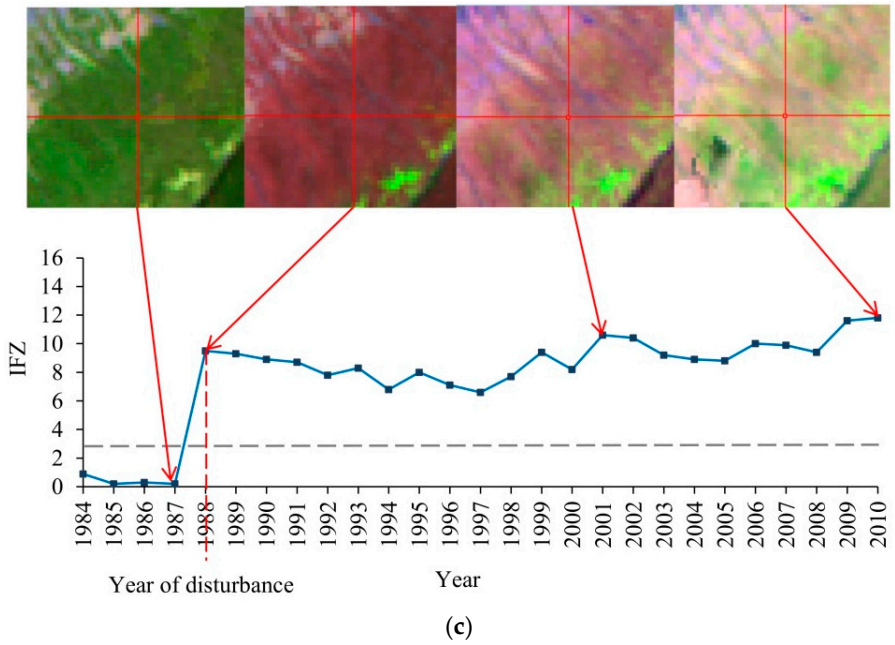

Figure 2. Examples showing where forest spectral recovery: occurred (**a**,**b**); and did not occur (**c**) following the 1988 Yellowstone fire as determined by tracking the IFZ values. (**a**,**b**) The disturbed pixels were reclassified as having forest cover by approximately 2003 and 2009, respectively. Each IFZ plot is for the center pixel, shown as the intersection of the two red lines in the images above it. The images are shown with bands 5, 4, and 3 displayed in red, green, and blue, respectively.

For Landsat TM and ETM images,

$$\text{NBR} = (\text{Band 4} - \text{Band 7})/(\text{Band 4} + \text{Band 7}), \quad (2)$$

$$\text{RdNBR} = (\text{prefireNBR} - \text{postfireNBR})/\sqrt{\text{ABS}\ (\text{prefireNBR}/1000)}, \quad (3)$$

where Band 4 is the Landsat red band and Band 7 is the Landsat near-infrared band. Threshold values of RdNBR were developed to classify fires across time and space in the US [66,67]. In this study, we adopted RdNBR thresholds for low-, medium-, and high-severity fires described in [66]. Percentage of forest recovery was then calculated by dividing the number of recovered pixels in the year 2011 (numerator) by the total number of disturbed pixels (denominator).

3.3. Validation of Recovery Products

We used the high-resolution images available from Google Earth to validate the RNR products at year 2011. By the time this study was conducted, Google Earth had acquired a comprehensive set of high-resolution images covering the study area in approximately 2011. With spatial resolutions of 1 m or better, these images allowed reliable determination of whether an area had tree cover through visual analysis. If at any specific validation point the available Google Earth images did not allow reliable visual analysis, ortho-photos acquired through the National Agricultural Imagery Program (NAIP) program were used to assist with the visual analysis (available online: http://www.fsa.usda.gov/).

Three steps were involved in the validation. First, based on forest type maps and burn severity maps, we randomly selected 100 pixels from each of the four major forest types (Lodgepole Pine, Whitebark Pine, Douglas-fir, and the combination of Engelmann Spruce and Subalpine Fir) and burn severities (low-, medium-, and high-severity fires) in the study region. Number of points sampled for each condition were shown in Table S1 in the Supplementary Materials. The forest type map was drafted before the 1988 fires and represented the forest conditions that were burned in 1988 (available

online: https://irma.nps.gov/App/Reference/Profile/1045509). Second, for each selected validation point, we divided the 30-m pixel equally with a 6 m by 6 m grid (25 cells in one 30-m pixel) and overlaid the grids onto the high-resolution images (Figure 3). Then, we counted the number of grids that was covered by trees and summed the percent tree cover by multiplying the number of forested grids by 4%, which is the area in percent of each grid (i.e., 1/25). Following the FAO forest definition (i.e., $\geq$10% tree cover), a disturbed pixel was considered to have recovered if the tree cover was at least 10% or more by 2011. Otherwise, that pixel was classified as having no detectable recovery. Third, we summarized the validation results to calculate the User's, Producer's and Overall Accuracies of the RNR products for fire and harvest and for each of the four forest types.

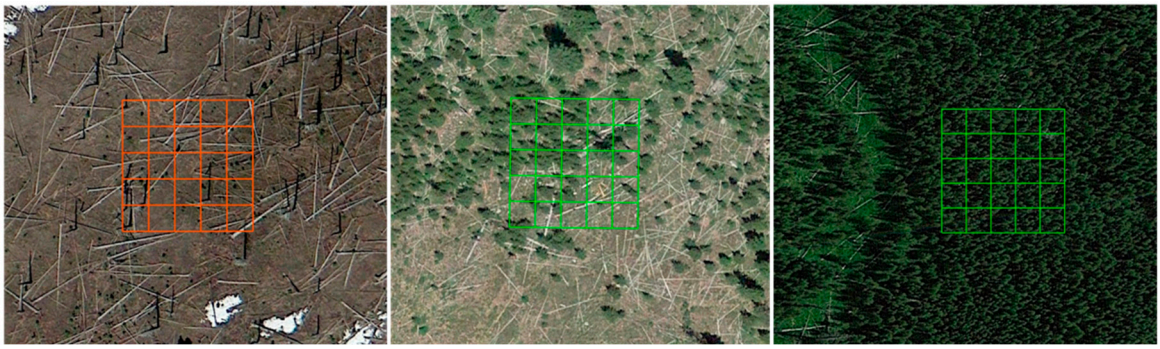

(**a**) (**b**) (**c**)

Figure 3. Examples of Google Earth validation of recovered and non-recovered pixels in 5 by 5 grids: (**a**) non-recovered; (**b**) recovered; and (**c**) recovered.

No design-based accuracy assessment was conducted for the years-until-detectable-recovery products because such an assessment would require annual high-resolution images at each selected validation location, which is unrealistic to collect. Instead, we did a qualitative assessment of this product using the Landsat images and the IFZ profiles, as shown in Figure 2, to verify that the VCT algorithm worked as designed in determining the years-until-detectable-recovery value.

3.4. Spatiotemporal Recovery Pattern Analysis

The maps produced in Section 3.2 provided the raw material used to evaluate the spatial and temporal patterns of forest recovery in the GYE. Global Moran's I values were calculated to determine whether any spatial clustering is present in the post-disturbance forest spectral recovery in the GYE. Global Moran's I is a measure of spatial autocorrelation and is characterized by a correlation in a signal among nearby locations in space [68,69]. To examine the spatial patterns of forest spectral recovery in the GYE, the fires, harvests and their associated recovery maps were overlaid with ownership boundary maps. For each disturbed pixel, we derived the annual forest recovery status by the end of the study interval. Then, we summarized the yearly percent forest recovery in the study area within the geographic area stratified by forest type and disturbance magnitude. Yearly percent forest recovery was calculated by dividing the number of recovered forest pixels by the number of total disturbed pixels.

We examined the spatial patterns of post-disturbance forest recovery in the GYE by calculating the number of years until a disturbed pixel spectrally recovered to forest. Lower numbers of years required for a pixel to recover indicate faster recoveries, and higher numbers indicate slower recoveries. For temporal analysis, we used the annual fire and harvest data from 1985 to 2011 to track long-term post-disturbance forest recovery in the GYE. We summarized the yearly percent forest recovery in the burned and harvested areas and compared the percent forest recovery following these two disturbance types.

4. Results

4.1. Accuracy of the Forest Spectral Recovery/No-Detectable-Recovery (RNR) Maps

The VCT RNR maps had overall accuracies of ~80% for different disturbance and forest types. In general, these accuracies were consistent among different disturbance types (Table 1) and forest types (Table 2), although recovery detection over harvested areas was slightly more accurate than over burned areas. Number of validation sampling points for each disturbance type and forest types were included in Tables S2 and S3, respectively. Errors were mainly associated with omitting pixels that had tree cover >10% by 2011, but were classified as no-detectable-recovery by VCT (omission errors of 13% for fire disturbances and 12% for harvests, respectively). The low Producer's Accuracy for the post-fire recovered class (producer's accuracy of 59%) suggest that the VCT forest recovery product underestimate the recovered class in the post-fire forest recovery, while the low User's Accuracy (user's accuracy of 58%) for the post-harvest no-detectable-recovery class indicate that VCT overestimate the no-detectable-recovery class and 42% of the "no-detectable-recovery" class from VCT have more than 10% of forest cover by year 2011.

Table 1. Validation accuracies of VCT post-fire and post-harvest spectral recovery products for all forest types in the GYE. Map refers to the VCT predicted disturbance class. User's Accuracy is the measure of commission error, while the Producer's Accuracy represents the omission error.

Post-Fire Spectral Recovery Validation Results					
		Reference			
		Recovered (Tree Cover > 10%)	**No-Detectable-Recovery (Tree Cover ≤ 10%)**	**Row Total**	**User's Accuracy**
Map	Spectrally recovered	0.19	0.07	0.26	0.75
	No-detectable-recovery	0.13	0.61	0.74	0.82
	Column total	0.32	0.68	1.00	
	Producer's Accuracy	0.59	0.90		
	Overall Accuracy		0.80		
Post-Harvest Spectral Recovery Validation Results					
		Reference			
		Recovered (Tree Cover > 10%)	**No-Detectable-Recovery (Tree Cover ≤ 10%)**	**Row Total**	**User's Accuracy**
Map	Spectrally recovered	0.69	0.02	0.71	0.97
	No-detectable-recovery	0.12	0.17	0.29	0.58
	Column total	0.81	0.19	1.00	
	Producer's Accuracy	0.85	0.89		
	Overall Accuracy		0.86		

The species-level post-forest recovery validation reveals more information regarding the algorithm performance under different site and vegetation conditions. Based on the forest types before the 1988 fires, we validated the VCT post-fire forest recovery product for the GYE following the 1988 fires. Because timber-managed forests are relatively uniform and homogenous, we did not analyze post-harvests for the GYE by forest type. Error matrices at the species level (Table 2) for the post-fire forest recovery reveal that the VCT has the highest producer's accuracies for the non-recovered class, ranging from 92% to 98% across all forest types. For the dominant Lodgepole Pine forests in YNP, the user's accuracy and overall accuracy of the VCT recovery product by year 2011 varies from 78% to 94%. Although the User's accuracy for the recovered class is less than 20%, the overall accuracy for Whitebark Pine forests remains over 85%, suggesting: (1) that the majority of burned Whitebark Pine pixels have not recovered from the fires and the overall accuracy of Whitebark Pine

forest recovery product relies heavily on the classification accuracy of the non-recovered class; and (2) that improvements are needed for the VCT algorithm to accurately track sparse and bright forest ecosystems at high elevations, such as the Whitebark Pine ecosystem.

For less common forest types, such as Douglas-fir, Engelmann Spruce and Subalpine Fir, the VCT also shows consistent accuracies for the rest of the YNP forests. The overall and user's accuracies for both forest types fluctuate by approximately 80%, with the main source of error stemming from omission errors for the recovered class. These results show that the VCT has high accuracy for the "no-detectable-recovery class but omits certain pixels that have already recovered from the fires, based on our forest definition discussed above.

Table 2. Validation accuracy of the VCT post-fire forest regrowth product for the four major forest species in YNP. Map refers to VCT predicted recovery class for each forest type. User's Accuracy is the measure of commission error, while the Producer's Accuracy represents the omission error.

Lodgepole Pine (72% of Area)					
		Reference			
		Recovered (Tree Cover > 10%)	**No-Detectable-Recovery (Tree Cover ≤ 10%)**	**Row Total**	**User's Accuracy**
Map	Spectrally recovered	0.28	0.02	0.30	0.94
	No-detectable-recovery	0.15	0.55	0.70	0.78
	Column total	0.43	0.57	1.00	
	Producer's Accuracy	0.65	0.97		
	Overall Accuracy		0.83		
Whitebark Pine (15% of Area)					
		Reference			
		Recovered (Tree Cover > 10%)	**No-Detectable-Recovery (Tree Cover ≤ 10%)**	**Row Total**	**User's Accuracy**
Map	Spectrally recovered	0.01	0.04	0.05	0.18
	No-detectable-recovery	0.08	0.87	0.95	0.92
	Column total	0.09	0.91	1.00	
	Producer's Accuracy	0.11	0.95		
	Overall Accuracy		0.88		
Douglas Fir (7.1% of Area)					
		Reference			
		Recovered (Tree Cover > 10%)	**No-Detectable-Recovery (Tree Cover ≤ 10%)**	**Row Total**	**User's Accuracy**
Map	Spectrally recovered	0.17	0.04	0.22	0.80
	No-detectable-recovery	0.19	0.59	0.78	0.75
	Column total	0.37	0.63	1.00	
	Producer's Accuracy	0.47	0.93		
	Overall Accuracy		0.76		
Engelmann Spruce and Subalpine Fir (5.9% of Area)					
		Reference			
		Recovered (Tree Cover > 10%)	**No-Detectable-Recovery (Tree Cover ≤ 10%)**	**Row Total**	**User's Accuracy**
Map	Spectrally recovered	0.03	0.02	0.05	0.68
	No-detectable-recovery	0.15	0.80	0.95	0.84
	Column total	0.18	0.82	1.00	
	Producer's Accuracy	0.18	0.98		
	Overall Accuracy		0.84		

4.2. Spectral Recovery Patterns by Ownership, Disturbance Type, Forest and Soil Types in the GYE

Spatial patterns of forest spectral recovery were summarized and analyzed following all disturbances occurring in the GYE before 2000 to allow enough time for forest spectral recover to occur (Figure 4). The Global Moran's I value of the forest spectral recovery map by year 2011 was

0.55, indicating that the forest recovery was highly clustered across the GYE. The main cluster of forest recovery in the GYE is distributed centrally around the boundary of Yellowstone National Park and Caribou-Targhee National Forest, where both large fires and intensive harvests occurred in the 1980s. For the 1988 Yellowstone Fire, this recovered clustering is largely located at lower elevations (<2300 m) where the growing season is longer and productivity is higher. Over 80% of the higher-elevation (>2300 m) burned area in Yellowstone National Park has not recovered from the 1988 fire. Post-fire forests in the national forests appear to have grown back faster than those in the national parks and wilderness area.

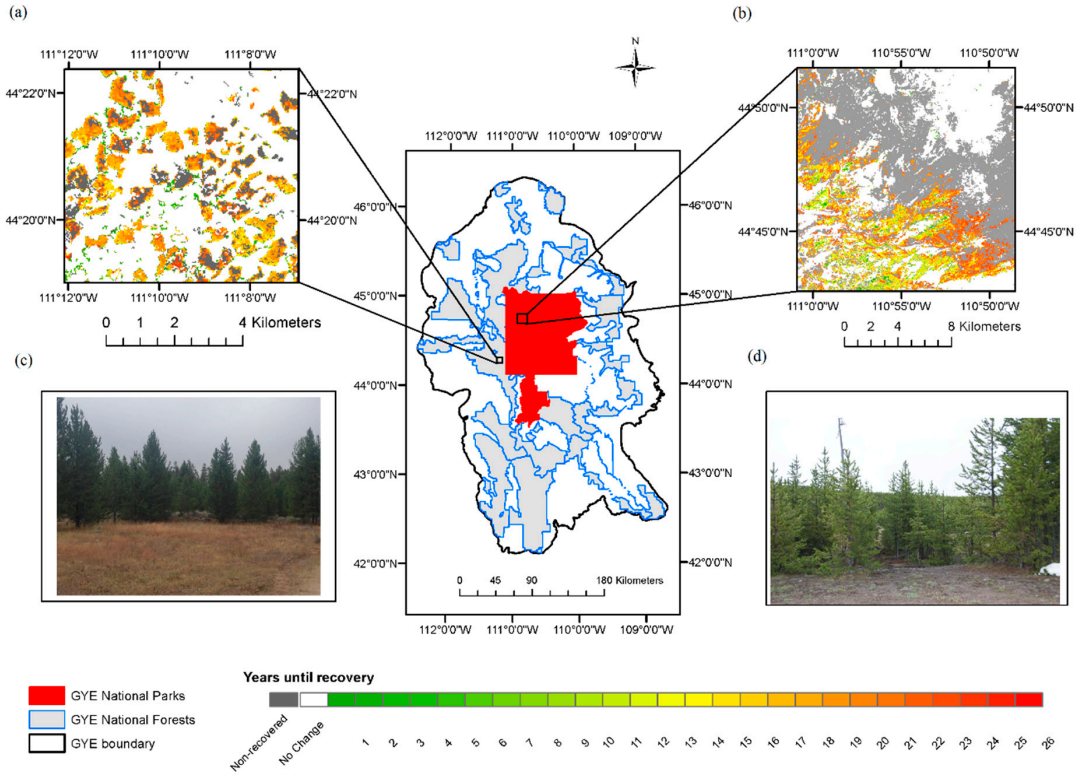

Figure 4. GYE forest spectral recovery from past disturbance maps and field photos. Only previously disturbed pixels were shown in the figure. Years-until-detectable-recovery indicates the number of years required for a pixel to regain identification as a forest following disturbance events based on the VCT time series recovery product. The grey color is the non-recovered area by 2011. (**a**) An example of forest spectral recovery following harvesting events in the Caribou-Targhee National Forest (near the boundary of YNP) in the 1980s; (**b**) an example of forest spectral recovery from the YNP 1988 fires; and (**c**,**d**) photographs of the current forest condition in the post-harvest and post-fire sites taken on 22 September 2013 and 17 May 2014, respectively.

Temporal patterns of forest recovery in the GYE were computed and summarized by disturbance type (Figure 5). Fires in the GYE are primarily infrequent high-severity fires with fire intervals ranging from 50 to 300 years [70,71]. We summarized the percent of forest recovery following two major fire years (year 1988 and year 1997) by land ownership in the GYE. The year 1988 represents a big fire year, whereas the year 1997 represents a relatively small fire year in the 1990s era. Although many fire years occurred in the 2000s, the recovery times following these fires were too short to show a forest spectral recovery trend. The long-term forest recoveries following the fires by ownership (Figure 5a,b) reveal that the post-fire forest recovery differed between the two fires years, and a longer recovery period did not necessarily result in higher recovery rates. After more than two decades of recovery, the percent of forest burned in 1988 that returned to forest by the year 2011 is quite low, even lower than the forest recovery rates by 2011 following the 1997 fires (Figure 5a,b).

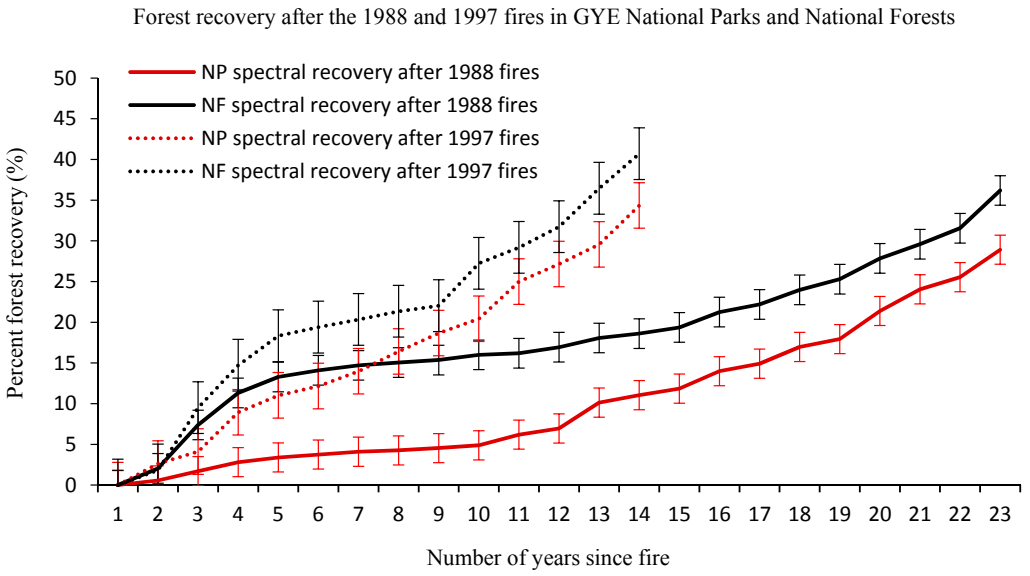

(**a**)

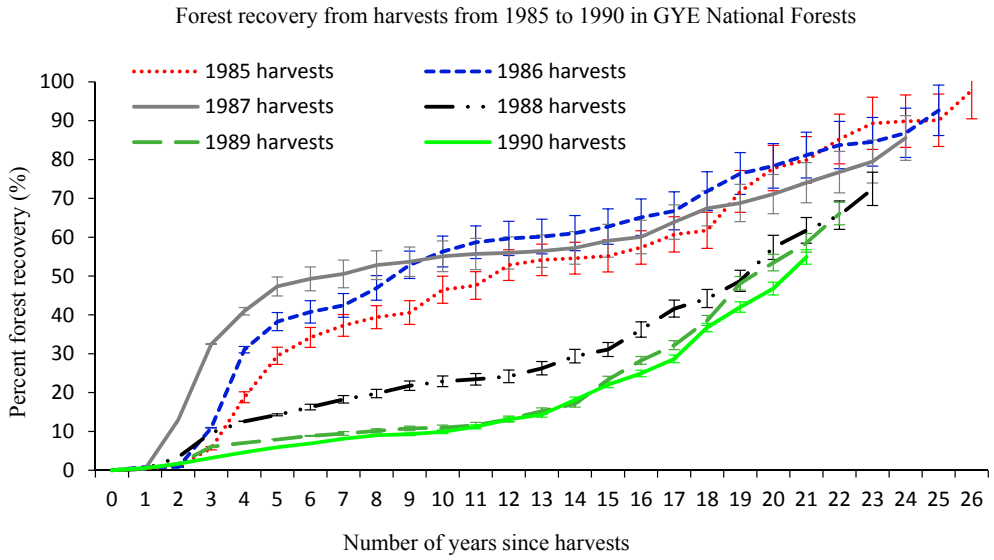

(**b**)

Figure 5. Temporal patterns of forest spectral recovery in the GYE by disturbance type. (**a**) Percentages of forest spectral recovery by ownership following the fires in 1988 and 1997 in the GYE. The long-term (>10 years) forest spectral recovery rates were highest on GYE national forest (NF, average elevation 2238 m) lands, followed by national parks (NP, average elevation 2435 m); (**b**) Percentages of forest spectral recovery following major harvesting years (1985 to 1990) in the GYE national forests (wilderness areas excluded). The slopes of the cumulative proportion lines indicate the rates of spectral recovery. Percentage of forest spectral recovery was calculated by dividing the number of recovered pixels in the year 2011 (numerator) by the total number of disturbed pixels (denominator). Error bars are 1 standard error.

The long-term GYE forest spectral recovery trend also differs by ownership. Affected by the differences in natural environmental conditions and human interferences (such as post-harvest planting), forests on national forest land generally grow back faster than forests in national parks and wilderness areas. During the two decades following the high magnitude fires in 1988, national forests consistently had higher values of forest spectral recovery than national parks and wilderness areas.

Despite the short-term similarity to the wilderness areas in the first few years after the 1997 fires, forest spectral recovery in the GYE national forests rapidly outpaced the rest of the GYE forests.

The recovery of the forests following major harvesting years in the GYE NFs (1985–1990, Figure 5b) exhibits the following trends. (1) The percentage of forest that recovered from a harvest in the GYE by year 2011 generally depends on the year of the harvest, and the recovery trajectory can be grouped into two recovery periods, the mid-1980s (1985–1987) and the late-1980s (1988–1990). (2) For harvests in mid-1980s, over 85% of the harvested area has returned to forest by 2011. Harvests that occurred in late-1980s have lower percentages of forest spectral recovery than the early years, and the spectral recovery trajectories differ between the two time periods. (3) For the earlier harvest period, two rapid spectral recovery intervals occurred in the early 1990s and mid-2000s. In contrast, for the late 1980s harvesting period, the average spectral recovery speed was slow for the first 15 years after the harvest, followed by rapid spectral recovery over the last decade.

Among different disturbance types, post-harvest forest spectral recovery rates are consistently higher than post-fire forest spectral recovery rates in the GYE. The percentages of forest spectral recovery reach 50%–90% following the 1980s' harvests, whereas the highest percent of forest spectral recovery following the 1988 fires is less than 40% by the year of 2011. Even only considering the national forest land, post-harvest forest spectral recovery rates (72% for harvests that occurred in 1988) are still much higher than the post-fire forest spectral recovery rates (36% for fires that occurred in 1988) by year 2011. Further investigation into the potential causes of different forest spectral recovery rates among different ownership and disturbance types is discussed in the following sections.

4.3. Spectral Recovery Patterns along Environmental Gradients in the Yellowstone National Park

Lodgepole Pine is the most dominant forest species in the Yellowstone National Park, covering over 70% of the forested area, followed by Whitebark Pine, Engelmann spruce and Subalpine Fir and Douglas fir (Figure 6a). The elevations these forest types inhabit also range from 1800 m to about 3000 m, ordered from low to high elevations are Douglas-fir, Lodgepole Pine, Engelmann Spruce and Subalpine Fir, and Whitebark Pine as the highest elevation forest ecosystem (Figure 6b). An examination of the spectral recovery percentages of major forest types in YNP following the 1988 fires (Figure 6c) shows that Whitebark Pine, Engelmann Spruce and Subalpine Fir at higher elevations have very low spectral recovery percentages (less than 10%). Lodgepole Pine has the highest percent of forest spectral recovery by 2011 (more than 30%), followed by Douglas-fir with more than 25% of the forest having spectrally recovered from the 1988 fires.

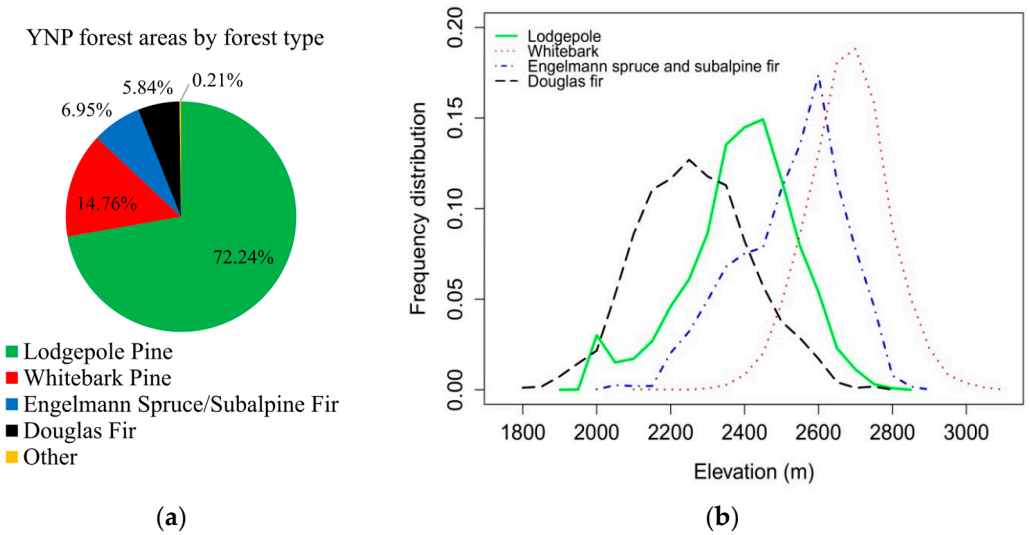

Figure 6. *Cont.*

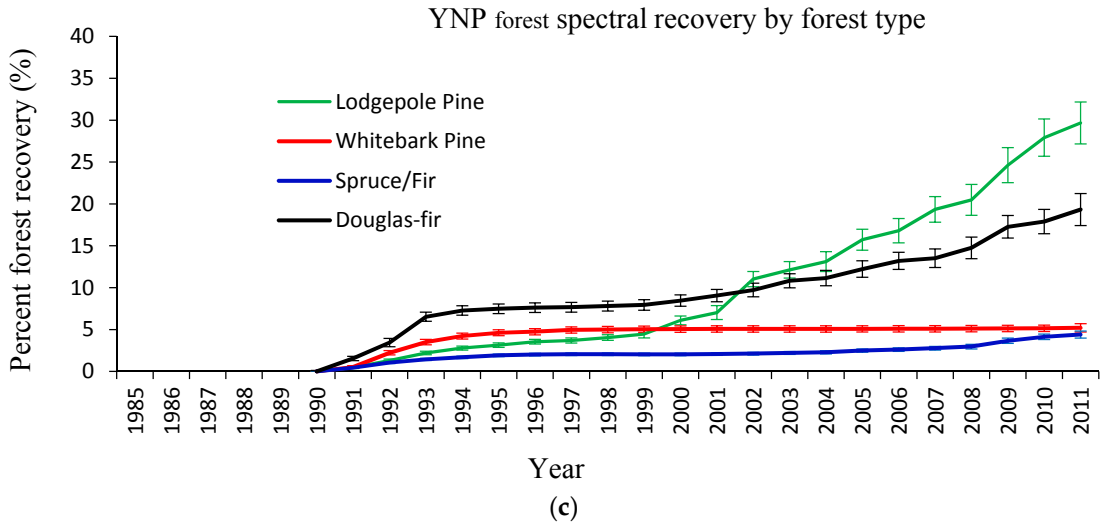

Figure 6. Forest species and spectral recovery percentages in Yellowstone National Park. (**a**) Forested area by forest type in Yellowstone National Park (before the 1988 fires); and (**b**) distributions of common tree species relative to elevation before the 1988 fires and percentages of forest spectral recovery by soil type after the 1988 fires in YNP. Engelmann Spruce and Subalpine Fir are found in the subalpine zone, but Whitebark pine is dominant at the upper end of this zone. Below the subalpine zone lies the montane zone, co-dominated by Douglas Fir (*Pseudotsuga menziesii*) at the lowest elevation zone and by Lodgepole Pine (*Pinus contorta*). Lodgepole Pine occupies a broad range of elevations and survives on drier, more exposed slopes with relatively poor substrates; (**c**) YNP forest spectral recovery after the 1988 fires separated by major forest types. The forest type map was drafted before the 1988 fires. Error bars are one standard error.

Soil compositions are also associated with post-fire long-term forest spectral recovery trends (Figure 7). Inceptisols, a relatively nutrient poor soil on which Lodgepole Pines mainly inhibat, had the lowest recovery rates before year 2000, but quickly caught up and become the soil type with the highest recovery rates by year 2011. Mollisols and mixed soil had steady increasing forest recovery rates; while the bed rock with soil had the highest spectral recovery rates during the study interval, possibly related to the quick recovery in some of the Douglas-fir forests growing in this soil type (Figure 7a).

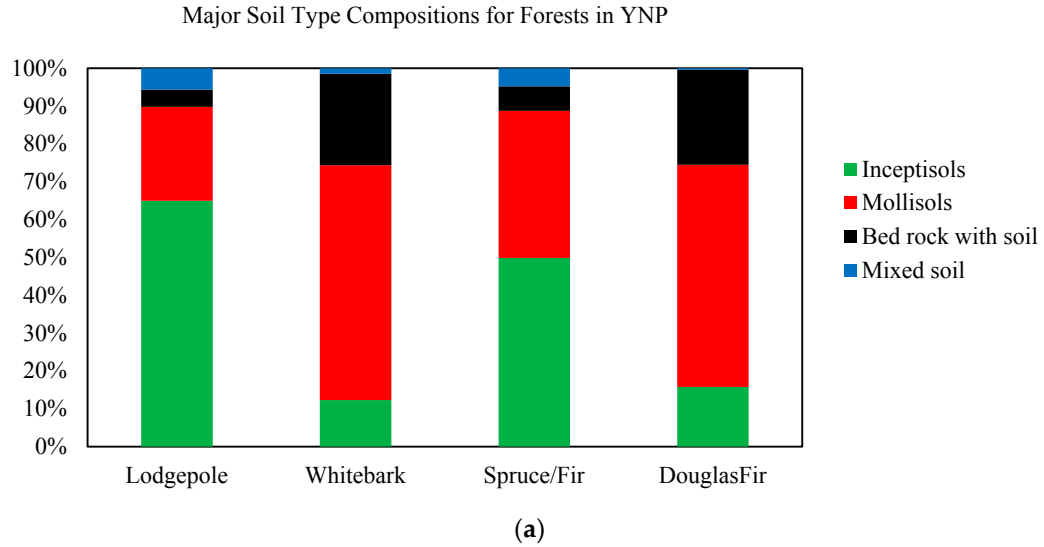

Figure 7. *Cont.*

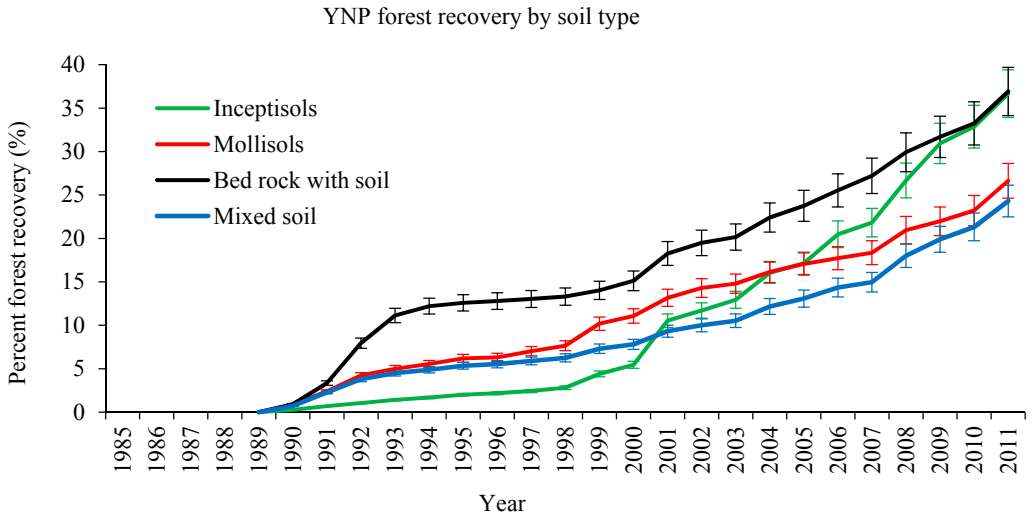

(**b**)

Figure 7. (**a**) Major soil types forests inhabit in Yellowstone National Park (YNP); and (**b**) percentages of forest spectral recovery for major soil types in YNP following the 1988 fires.

5. Discussion

Studies of disturbance events in the GYE forest catalyzed recognition of the importance of large-scale disturbances and regrowth as key drivers of carbon fluxes in terrestrial ecosystems [71]. The disturbance and regrowth patterns in the GYE underscored the importance of environmental variables (such as substrate and topography) in ecosystem responses to disturbance. This study assessed the usefulness of time series composed of Landsat images and the VCT in tracking post-fire and post-harvest forest spectral recovery in the GYE. The VCT algorithm was found to be effective in tracking forest spectral recovery through time in the GYE. In this study, we used the LTSS-VCT approach to map forest spectral recovery following these disturbances and conducted a comprehensive assessment of the derived spectral recovery products. The validated spectral recovery products were then used to quantify patterns and rates of forest spectral recovery following major fires and logging activities. In addition, the results from such an assessment is valuable and informative for many ecological studies and can be used to inform management decision making regarding ecosystem conservation, biodiversity protection, and carbon sequestration [72]. Many ecosystem models assume post-disturbance forest recovery occurs immediately or homogenously across the landscape. It is observed in this study, however, forest spectral recovery does not always occur immediately or homogenously after disturbances. Take the 1988 fires as an example—24 years after the fires, over 50% of the burned area still do not have recovered to the point that can be detected by remote sensing, and burned areas with higher elevations are seeing much lower spectral recovery percentages than those in lower elevations. This finding has important ecological implications and could potentially change the way many ecosystem models simulate post-disturbance forest regrowth.

5.1. Challenges in Time Series Forest Recovery Mapping

The VCT algorithm recorded a total of 5341 km^2 of fire disturbances and 953 km^2 of harvesting in the GYE forests from 1985 to 2011. A comparison with point-based interpretations from TimeSync showed that the VCT fire detection was highly reliable, with a user's accuracy of 96% and a producer's accuracy of 73% [2]. The VCT's detection of high- and moderate-severity fires is highly successful, and most of the omission errors were from low-severity fires. The accuracy of the estimated forest loss due to harvesting was also high, with a user's accuracy of 91% and a producer's accuracy of 89% [2].

Certain uncertainties and limitations are present in the study. Insufficient ground data, limited mapping capabilities and inadequate scientific understanding of the complex interactions between natural phenomena may have generated uncertainty in this study. With proper quality control in the validation process, the uncertainties in this assessment are limited to the biophysical map input and the methods related to forest regrowth modeling. The known limitations of this approach include the following: (1) The VCT algorithm is not sensitive to low-severity disturbances and may miss some low-intensity forest loss [2,45]. In this study, for example, some of the low severity fires and partial harvests were not mapped and the recovery following these low intensity disturbances might not be fully understood; (2) Temporal accuracy were not validated. Due to the lack of time series high spatial resolution images covering the whole region, we focused on validating the forest recovery status mapped by VCT around year 2011. Although the VCT algorithm has been proven effective to separate forest from non-forest land cover types in previous literature, the lack of fully assessed temporal accuracy could still reduce the reliability of the temporal analysis; (3) Spectral recovery characterized in this study is different than stand recovery, which is measured in stand structure such as height or biomass and is the indication for true forest recovery [73–75], while spectral recovery used in this study is measured by how closely spectral vectors match pre-disturbance spectral vectors, and the spectral index used to model the recovery affects the outcomes of the results [76,77].

The VCT algorithm was able to accurately capture forest spectral recovery at the regional level, but there are still certain issues to solve at the species level. For dominant species at moderate elevations, such as Lodgepole Pine and Douglas-fir, the performance of the algorithm is consistent and reliable. However, the algorithm might need to be adjusted for high-elevation forest types, such as Whitebark Pine, Engelmann Spruce and Subalpine Fir, because of the different forest structure and spectral characteristics of the high-elevation forest ecosystems. The compositing and cloud masking algorithm might not work very well in sparse vegetation, and could potentially contribute to mapping errors in these regions.

Some studies also include minimum tree height as part of their forest and forest recovery definition [7]. In this study, however, minimum tree height was not included because we followed the FAO forest definition that trees should be able to reach a minimum height of 5 m at maturity in situ (FAO 1998). Even if there are only small trees on the ground, it should still be called a forest by this definition. Turner et al. [42] used long term plot data to examine long term forest recovery in GYE also found that post-fire stand structure and function recovery did not converge simultaneously, but stand function will converge sooner than structure [42].

5.2. Spatial and Temporal Pattern Analysis of Forest Spectral Recovery in the GYE

Forest spectral recovery rates following fires in different years can vary based on different regeneration conditions, such as seed availability and post-disturbance climate conditions [78,79]. By 2011, the forest spectral recovery rates following the 1988 fires were lower than those of the 1997 for national parks and national forests. Several potential contributing factors include the following. (1) Seed bank availability is lower for big fires; therefore, the large burned areas in 1988 required a longer time to recover than the smaller fires in 1997, especially for colonizing species such as Douglas-fir [80]; (2) Previous studies suggested that post-fire climate could have a significant impact on forest recovery [23]. Post-fire precipitation was higher for the 1997 fires than that of the 1988 fires in the GYE. The three-year mean annual precipitation following the 1988 fires (205 mm) was much lower than that following the 1997 fires (249 mm), producing less ideal conditions for forest regeneration. Similarly for the post-harvest forest recovery, post-harvest climate also played an important role in forest recovery before and after 1988. Year 1987 and 1988 were both severe drought years in the GYE [81], compared with climatically normal years of 1985 and 1986, which could possibly explain the diverging post-harvest recovery trends before and after 1988.

Spectral recovery tends to occur fairly quickly (within 5–15 years depending on the forest type), and even low biomass levels may lead to IFZ values comparable to those of mature forests [43,82].

For both post-fire and post-harvest forest spectral recovery, we see gentle spikes of forest recovery in the first decade following the disturbance. This immediate increase in forest recovery could be caused by the following reasons: (1) the quick recovery of understory grass and shrubs that increases forest indices to levels close to the forest level; and/or (2) the failure of low- and moderate-severity fires to kill all the trees; the survivors then green up in the following years, saturate the spectral information, and cause VCT to misclassify spectral forest recovery. However, during the validation process, we noticed that over 80% of the validated "no-detectable-recovery" plots have sparse saplings growing back, but not to the level that can be detected at a resolution of 30 m. The saplings within 1 Landsat pixel are either too small or too sparse to be detected at this scale.

Lodgepole Pines, the main forest species in the Yellowstone National Park, are known to have fire adapted traits such as serotinous cones and prolific seeding [51,83]. Previous field measurement based studies in GYE revealed that seed released from serotinous Lodgepole Pines determine the initial postfire Lodgepole regeneration, and stem density is highly depend on the prefire prevalence of serotiny [42,55,84]. Long term forest recruitment, however, depends on seed release from non-serotinous cones, which contributes as seed source for infilling [42].

Fire severity has been suggested to have substantial effects on early post-fire plant cover and species richness in Yellowstone National Parks [55,84]. Our results reveal that fire severity did not show significant impact on long-term forest recovery by the year 2011 (Figure 8), whereas the effects of environmental variations were more pronounced [56,71]. For the VCT mapped "non-recovered" class, the mean canopy cover for all burn severities were less than 10%, with slightly higher mean canopy cover following the low severity fires. In the VCT mapped "recovered" class, all mean canopy cover are greater than 50%, with higher canopy cover in moderate and high severity fire categories. This might relate to the fact that Lodgepole Pines have serotinous cones that are adapted to stand replacing fires. Field-based studies in Yellowstone National Park also suggested that the abundance and spatial distributions of surviving trees and seedlings may be the pivotal factors determining early forest regrowth following disturbances [42,85].

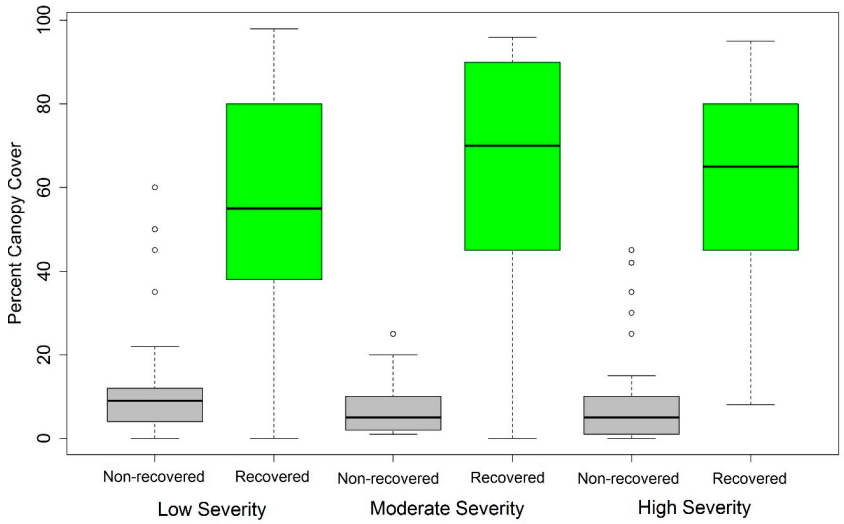

Figure 8. Canopy cover following low, moderate and high severity fires in VCT mapped spectrally non-recovered (grey color) and spectrally recovered (green color) classes. The results were summarized from high resolution validation points stratified by burn severity and recover status.

6. Conclusions

In summary, the results from this study underscore the ability of the VCT algorithm to monitor large-scale time series data on forest spectral recovery associated with multiple disturbance types. Based on the temporal and spatial consistency, we characterized the temporal forest spectral recovery

history in the GYE using the VCT forest spectral recovery data. We analyzed the spatial and temporal forest spectral recovery trends in the GYE with respect to different land ownership (management regimes), disturbance types, and forest types. With the public availability of VCT disturbance and recovery products nationwide (available online: https://daac.ornl.gov/cgi-bin/dsviewer.pl?ds_id=1290), this approach can be applied to other regions of the U.S. for many other monitoring and management purposes.

Supplementary Materials: The following are available online at www.mdpi.com/2072-4292/8/11/898/s1, Table S1: Number of validation points for post-fire forest recovery in the study region, stratified by forest species, burn severity, and recovery status, Table S2: Number of sampling points and accuracy assessment for validating VCT (a) post-fire and (b) post-harvest spectral recovery products for all forest species in the GYE. Map refers to the VCT predicted disturbance class, Table S3: Number of sampling points and validation accuracy of the VCT post-fire forest spectral recovery product for the four major forest species in YNP. Map refers to VCT predicted spectral recovery class for each forest type, Table S4: Maximum IFZ (Integrated Forest z-score) values and minimum NDVI (Normalized Difference of Vegetation Index) values used to determine forest spectral recovery in GYE.

Acknowledgments: This study was supported by funding from the USGS LANDCarbon project. The authors would like to thank Google Earth for providing the validation platform. Roy Renkin and Carrie Guiles from the National Park Service, Yellowstone National Park kindly shared their rich knowledge on YNP and provided data assistance. The authors would also like to thank Kate Rice, Ashwan Reddy, and Cheryl Nichols for proof-reading the manuscript and providing lots of helpful writing suggestions.

Author Contributions: Feng Robin Zhao, Ran Meng, Chengquan Huang, and Zhiliang Zhu conceived the idea and designed the methodology; Feng Robin Zhao, Ran Meng, Maosheng Zhao, and Feng Aron Zhao performed the data analysis; and Feng Robin Zhao, Ran Meng, Chengquan Huang, Peng Gong, Le Yu, and Zhiliang Zhu prepared manuscripts and contributed to the discussion.

Conflicts of Interest: The authors declare no conflict of interest.

Abbreviations

The following abbreviations are used in this manuscript:

GYE	Greater Yellowstone Ecosystem
YNP	Yellowstone National Park
NPs	National Parks
NFs	National Forests
WAs	Wilderness Areas
VCT	Vegetation Change Tracker
IFZ	Integrated Forest z-score

References

1. Parmenter, A.W.; Hansen, A.; Kennedy, R.E.; Cohen, W.; Langner, U.; Lawrence, R.; Maxwell, B.; Gallant, A.; Aspinall, R. Land use and land cover change in the greater yellowstone ecosystem: 1975–1995. *Ecol. Appl.* **2003**, *13*, 687–703. [CrossRef]
2. Zhao, F.; Huang, C.; Zhu, Z. Use of vegetation change tracker and support vector machine to map disturbance types in greater yellowstone ecosystems in a 1984–2010 Landsat time series. *IEEE Geosci. Remote Sens. Lett.* **2015**, *12*, 1650–1654. [CrossRef]
3. Pan, Y.; Birdsey, R.A.; Fang, J.; Houghton, R.; Kauppi, P.E.; Kurz, W.A.; Phillips, O.L.; Shvidenko, A.; Lewis, S.L.; Canadell, J.G. A large and persistent carbon sink in the world's forests. *Science* **2011**, *333*, 988–993. [CrossRef] [PubMed]
4. Houghton, R.A.; Hackler, J.L.; Lawrence, K. The us carbon budget: Contributions from land-use change. *Science* **1999**, *285*, 574–578. [CrossRef] [PubMed]
5. Goetz, S.J.; Bond-Lamberty, B.; Law, B.E.; Hicke, J.; Huang, C.; Houghton, R.; McNulty, S.; O'Halloran, T.; Harmon, M.; Meddens, A. Observations and assessment of forest carbon dynamics following disturbance in North America. *J. Geophys. Res. Biogeosci.* **2012**, *117*, 1–17. [CrossRef]
6. Liu, S.; Bond-Lamberty, B.; Hicke, J.; Vargas, R.; Zhao, S.; Chen, J.; Edburg, S.; Hu, Y.; Liu, J.; McGuire, A.; et al. Simulating the impacts of disturbances on forest carbon cycling in North America: Processes, data, models, and challenges. *J. Geophys. Res. Biogeosci.* **2011**, *116*, 1–22. [CrossRef]

7. Bartels, S.F.; Chen, H.Y.H.; Wulder, M.A.; White, J.C. Trends in post-disturbance recovery rates of Canada's forests following wildfire and harvest. *For. Ecol. Manag.* **2016**, *361*, 194–207. [CrossRef]
8. Schroeder, T.A.; Cohen, W.B.; Yang, Z. Patterns of forest regrowth following clearcutting in western Oregon as determined from a Landsat time-series. *For. Ecol. Manag.* **2007**, *243*, 259–273. [CrossRef]
9. Potter, C.; Li, S.; Huang, S.; Crabtree, R.L. Analysis of sapling density regeneration in Yellowstone National Park with hyperspectral remote sensing data. *Remote Sens. Environ.* **2012**, *121*, 61–68. [CrossRef]
10. Frolking, S.; Palace, M.W.; Clark, D.B.; Chambers, J.Q.; Shugart, H.H.; Hurtt, G.C. Forest disturbance and recovery: A general review in the context of spaceborne remote sensing of impacts on aboveground biomass and canopy structure. *J. Geophys. Res. Biogeosci.* **2009**, *114*, 1–27. [CrossRef]
11. Kennedy, R.E.; Yang, Z.; Cohen, W.B.; Pfaff, E.; Braaten, J.; Nelson, P. Spatial and temporal patterns of forest disturbance and regrowth within the area of the Northwest Forest plan. *Remote Sens. Environ.* **2012**, *122*, 117–133. [CrossRef]
12. Vogelmann, J.E.; Gallant, A.L.; Shi, H.; Zhu, Z. Perspectives on monitoring gradual change across the continuity of Landsat sensors using time-series data. *Remote Sens. Environ.* **2016**, *185*, 258–270. [CrossRef]
13. Vogelmann, J.E.; Xian, G.; Homer, C.; Tolk, B. Monitoring gradual ecosystem change using Landsat time series analyses: Case studies in selected forest and rangeland ecosystems. *Remote Sens. Environ.* **2012**, *122*, 92–105. [CrossRef]
14. Hansen, M.C.; Potapov, P.V.; Moore, R.; Hancher, M.; Turubanova, S.; Tyukavina, A.; Thau, D.; Stehman, S.; Goetz, S.; Loveland, T. High-resolution global maps of 21st-century forest cover change. *Science* **2013**, *342*, 850–853. [CrossRef] [PubMed]
15. Lentile, L.B.; Holden, Z.A.; Smith, A.M.S.; Falkowski, M.J.; Hudak, A.T.; Morgan, P.; Lewis, S.A.; Gessler, P.E.; Benson, N.C. Remote sensing techniques to assess active fire characteristics and post-fire effects. *Int. J. Wildland Fire* **2006**, *15*, 319–345. [CrossRef]
16. Chu, T.; Guo, X. Remote sensing techniques in monitoring post-fire effects and patterns of forest recovery in boreal forest regions: A review. *Remote Sens.* **2013**, *6*, 470–520. [CrossRef]
17. Tanase, M.; de la Riva, J.; Santoro, M.; Pérez-Cabello, F.; Kasischke, E. Sensitivity of sar data to post-fire forest regrowth in Mediterranean and boreal forests. *Remote Sens. Environ.* **2011**, *115*, 2075–2085. [CrossRef]
18. Kane, V.R.; North, M.P.; Lutz, J.A.; Churchill, D.J.; Roberts, S.L.; Smith, D.F.; McGaughey, R.J.; Kane, J.T.; Brooks, M.L. Assessing fire effects on forest spatial structure using a fusion of Landsat and airborne lidar data in Yosemite National Park. *Remote Sens. Environ.* **2014**, *151*, 89–101. [CrossRef]
19. Asner, G.P.; Knapp, D.E.; Broadbent, E.N.; Oliveira, P.J.C.; Keller, M.; Silva, J.N. Selective logging in the Brazilian Amazon. *Science* **2005**, *310*, 480–482. [CrossRef] [PubMed]
20. Souza, C.M.; Roberts, D.A.; Cochrane, M.A. Combining spectral and spatial information to map canopy damage from selective logging and forest fires. *Remote Sens. Environ.* **2005**, *98*, 329–343. [CrossRef]
21. Andersen, H.-E.; Reutebuch, S.E.; McGaughey, R.J.; D'Oliveira, M.V.N.; Keller, M. Monitoring selective logging in western Amazonia with repeat lidar flights. *Remote Sens. Environ.* **2014**, *151*, 157–165. [CrossRef]
22. Schroeder, T.A.; Wulder, M.A.; Healey, S.P.; Moisen, G.G. Detecting post-fire salvage logging from Landsat change maps and national fire survey data. *Remote Sens. Environ.* **2012**, *122*, 166–174. [CrossRef]
23. Meng, R.; Dennison, P.E.; Huang, C.; Moritz, M.A.; D'Antonio, C. Effects of fire severity and post-fire climate on short-term vegetation recovery of mixed-conifer and red fir forests in the Sierra Nevada mountains of California. *Remote Sens. Environ.* **2015**, *171*, 311–325. [CrossRef]
24. Roy, D.P.; Wulder, M.A.; Loveland, T.R.; Woodcock, C.E.; Allen, R.G.; Anderson, M.C.; Helder, D.; Irons, J.R.; Johnson, D.M.; Kennedy, R. Landsat-8: Science and product vision for terrestrial global change research. *Remote Sens. Environ.* **2014**, *145*, 154–172. [CrossRef]
25. Zhu, Z.; Woodcock, C.E. Continuous change detection and classification of land cover using all available Landsat data. *Remote Sens. Environ.* **2014**, *144*, 152–171. [CrossRef]
26. Cohen, W.B.; Yang, Z.; Stehman, S.V.; Schroeder, T.A.; Bell, D.M.; Masek, J.G.; Huang, C.; Meigs, G.W. Forest disturbance across the conterminous united states from 1985–2012: The emerging dominance of forest decline. *For. Ecol. Manag.* **2016**, *360*, 242–252. [CrossRef]
27. Gong, P.; Xu, B. Remote sensing of forests over time. In *Remote Sensing of Forest Environments*; Springer: Boston, MA, USA, 2003; pp. 301–333.
28. Healey, S.P.; Cohen, W.B.; Zhiqiang, Y.; Krankina, O.N. Comparison of tasseled cap-based Landsat data structures for use in forest disturbance detection. *Remote Sens. Environ.* **2005**, *97*, 301–310. [CrossRef]

29. Schroeder, T.A.; Wulder, M.A.; Healey, S.P.; Moisen, G.G. Mapping wildfire and clearcut harvest disturbances in boreal forests with Landsat time series data. *Remote Sens. Environ.* **2011**, *115*, 1421–1433. [CrossRef]
30. Hilker, T.; Wulder, M.A.; Coops, N.C.; Linke, J.; McDermid, G.; Masek, J.G.; Gao, F.; White, J.C. A new data fusion model for high spatial- and temporal-resolution mapping of forest disturbance based on Landsat and MODIS. *Remote Sens. Environ.* **2009**, *113*, 1613–1627. [CrossRef]
31. Griffiths, P.; Kuemmerle, T.; Baumann, M.; Radeloff, V.C.; Abrudan, I.V.; Lieskovsky, J.; Munteanu, C.; Ostapowicz, K.; Hostert, P. Forest disturbances, forest recovery, and changes in forest types across the Carpathian ecoregion from 1985 to 2010 based on Landsat image composites. *Remote Sens. Environ.* **2014**, *151*, 72–88. [CrossRef]
32. Hermosilla, T.; Wulder, M.A.; White, J.C.; Coops, N.C.; Hobart, G.W.; Campbell, L.B. Mass data processing of time series Landsat imagery: Pixels to data products for forest monitoring. *Int. J. Digit. Earth* **2016**, *9*, 1–20. [CrossRef]
33. Huang, C.; Kim, S.; Altstatt, A.; Townshend, J.R.G.; Davis, P.; Song, K.; Tucker, C.J.; Rodas, O.; Yanosky, A.; Clay, R.; et al. Rapid loss of Paraguay's Atlantic forest and the status of protected areas—A Landsat assessment. *Remote Sens. Environ.* **2007**, *106*, 460–466. [CrossRef]
34. Potapov, P.; Hansen, M.C.; Stehman, S.V.; Pittman, K.; Turubanova, S. Gross forest cover loss in temperate forests: Biome-wide monitoring results using MODIS and Landsat data. *J. Appl. Remote Sens.* **2009**, *3*, 033569. [CrossRef]
35. Wulder, M.; White, J.; Alvarez, F.; Han, T.; Rogan, J.; Hawkes, B. Characterizing boreal forest wildfire with multi-temporal Landsat and lidar data. *Remote Sens. Environ.* **2009**, *113*, 1540–1555. [CrossRef]
36. Verbesselt, J.; Hyndman, R.; Newnham, G.; Culvenor, D. Detecting trend and seasonal changes in satellite image time series. *Remote Sens. Environ.* **2010**, *114*, 106–115. [CrossRef]
37. DeVries, B.; Verbesselt, J.; Kooistra, L.; Herold, M. Robust monitoring of small-scale forest disturbances in a tropical montane forest using Landsat time series. *Remote Sens. Environ.* **2015**, *161*, 107–121. [CrossRef]
38. Zhu, Z.; Woodcock, C.E.; Olofsson, P. Continuous monitoring of forest disturbance using all available Landsat imagery. *Remote Sens. Environ.* **2012**, *122*, 75–91. [CrossRef]
39. Baumann, M.; Ozdogan, M.; Kuemmerle, T.; Wendland, K.J.; Esipova, E.; Radeloff, V.C. Using the Landsat record to detect forest-cover changes during and after the collapse of the Soviet Union in the temperate zone of European Russia. *Remote Sens. Environ.* **2012**, *124*, 174–184. [CrossRef]
40. Kennedy, R.E.; Yang, Z.; Cohen, W.B. Detecting trends in forest disturbance and recovery using yearly Landsat time series: 1. LandTrendr—Temporal segmentation algorithms. *Remote Sens. Environ.* **2010**, *114*, 2897–2910. [CrossRef]
41. Trumbore, S.; Brando, P.; Hartmann, H. Forest health and global change. *Science* **2015**, *349*, 814–818. [CrossRef] [PubMed]
42. Turner, M.G.; Whitby, T.G.; Tinker, D.B.; Romme, W.H. Twenty-four years after the Yellowstone fires: Are postfire lodgepole pine stands converging in structure and function? *Ecology* **2016**, *97*, 1260–1273. [CrossRef] [PubMed]
43. Huang, C.; Goward, S.N.; Masek, J.G.; Thomas, N.; Zhu, Z.; Vogelmann, J.E. An automated approach for reconstructing recent forest disturbance history using dense Landsat time series stacks. *Remote Sens. Environ.* **2010**, *114*, 183–198. [CrossRef]
44. Huang, C.; Goward, S.N.; Masek, J.G.; Gao, F.; Vermote, E.F.; Thomas, N.; Schleeweis, K.; Kennedy, R.E.; Zhu, Z.; Eidenshink, J.C. Development of time series stacks of landsat images for reconstructing forest disturbance history. *Int. J. Digit. Earth* **2009**, *2*, 195–218. [CrossRef]
45. Thomas, N.E.; Huang, C.; Goward, S.N.; Powell, S.; Rishmawi, K.; Schleeweis, K.; Hinds, A. Validation of North American forest disturbance dynamics derived from Landsat time series stacks. *Remote Sens. Environ.* **2011**, *115*, 19–32. [CrossRef]
46. Huang, C.; Schleeweis, K.; Thomas, N.; Goward, S.N. Forest dynamics within and around the Olympic National Park assessed using time series Landsat observations. In *Remote Sensing of Protected Lands*; Wang, Y., Ed.; Taylor & Francis: London, UK, 2011; pp. 71–93.
47. Huang, C.; Goward, S.N.; Schleeweis, K.; Thomas, N.; Masek, J.G.; Zhu, Z. Dynamics of national forests assessed using the Landsat record: Case studies in eastern U.S. *Remote Sens. Environ.* **2009**, *113*, 1430–1442. [CrossRef]

48. Huang, C.; Ling, P.-Y.; Zhu, Z. North Carolina's forest disturbance and timber production assessed using time series Landsat observations. *Int. J. Digit. Earth* **2015**, *8*, 1–41. [CrossRef]
49. Landenburger, L.; Lawrence, R.L.; Podruzny, S.; Schwartz, C.C. Mapping regional distribution of a single tree species: Whitebark pine in the greater Yellowstone ecosystem. *Sensors* **2008**, *8*, 4983–4994. [CrossRef]
50. Alexander, R.R. Silviculture of central and southern Rocky Mountain forests: A summary of the status of our knowledge by timber types. In *Silviculture of Subalpine Forests in the Central and Southern Rocky Mountains: The Status of Our Knowledge*; Rocky Mountain Forest and Range Experiment Station: Fort Collins, CO, USA, 1974; pp. 1–35.
51. Alexander, R.R.; Edminster, C.B. Lodgepole pine management in the central Rocky mountains. *J. For.* **1980**, *78*, 196–201.
52. Hansen, A.J.; Rotella, J.J.; Kraska, M.P.; Brown, D. Spatial patterns of primary productivity in the greater Yellowstone ecosystem. *Lands. Ecol.* **2000**, *15*, 505–522. [CrossRef]
53. Robichaud, P.R.; Beyers, J.L.; Neary, D.G. *Evaluating the Effectiveness of Postfire Rehabilitation Treatments*; U.S. Department of Agricul, Forest Service: Fort Collins, CO, USA, 2000; p. 85.
54. Harvey, B.J.; Donato, D.C.; Romme, W.H.; Turner, M.G. Fire severity and tree regeneration following bark beetle outbreaks: The role of outbreak stage and burning conditions. *Ecol. Appl.* **2014**, *24*, 1608–1625. [CrossRef]
55. Turner, M.G.; Romme, W.H.; Gardner, R.H.; Hargrove, W.W. Effects of fire size and pattern on early succession in Yellowstone National Park. *Ecol. Monogr.* **1997**, *67*, 411–433. [CrossRef]
56. Franks, S.; Masek, J.G.; Turner, M.G. Monitoring forest regrowth following large scale fire using satellite data—A case study of Yellowstone National Park, USA. *Eur. J. Remote Sens.* **2013**, *46*, 551–569. [CrossRef]
57. Schoennagel, T.; Turner, M.G.; Romme, W.H. The influence of fire interval and serotiny on postfire lodgepole pine density in Yellowstone National Park. *Ecology* **2003**, *84*, 2967–2978. [CrossRef]
58. Romme, W.H.; Boyce, M.S.; Gresswell, R.; Merrill, E.H.; Minshall, G.W.; Whitlock, C.; Turner, M.G. Twenty years after the 1988 Yellowstone fires: Lessons about disturbance and ecosystems. *Ecosystems* **2011**, *14*, 1196–1215. [CrossRef]
59. Marston, R.A.; Anderson, J.E. Watersheds and vegetation of the greater Yellowstone ecosystem. *Conserv. Biol.* **1991**, *5*, 338–346. [CrossRef]
60. Renkin, R.A.; Despain, D.G. Fuel moisture, forest type, and lightning-caused fire in Yellowstone National Park. *Can. J. For. Res.* **1992**, *22*, 37–45. [CrossRef]
61. Masek, J.G.; Vermote, E.F.; Saleous, N.E.; Wolfe, R.; Hall, F.G.; Huemmrich, K.F.; Gao, F.; Kutler, J.; Lim, T.-K. A Landsat surface reflectance dataset for North America, 1990–2000. *IEEE Geosci. Remote Sens. Lett.* **2006**, *3*, 68–72. [CrossRef]
62. Huang, C.; Thomas, N.; Goward, S.N.; Masek, J.G.; Zhu, Z.; Townshend, J.R.; Vogelmann, J.E. Automated masking of cloud and cloud shadow for forest change analysis using Landsat images. *Int. J. Remote Sens.* **2010**, *31*, 5449–5464. [CrossRef]
63. Huete, A.R.; Liu, H.Q.; Batchily, K.; van Leeuwen, W. A comparison of vegetation indices over a global set of TM images for EOS-MODIS. *Remote Sens. Environ.* **1997**, *59*, 440–451. [CrossRef]
64. Kogan, F. Application of vegetation index and brightness temperature for drought detection. *Adv. Space Res.* **1995**, *15*, 91–100. [CrossRef]
65. Huang, C.; Song, K.; Kim, S.; Townshend, J.R.G.; Davis, P.; Masek, J.; Goward, S.N. Use of a dark object concept and support vector machines to automate forest cover change analysis. *Remote Sens. Environ.* **2008**, *112*, 970–985. [CrossRef]
66. Miller, J.D.; Thode, A.E. Quantifying burn severity in a heterogeneous landscape with a relative version of the delta normalized burn ratio (DNBR). *Remote Sens. Environ.* **2007**, *109*, 66–80. [CrossRef]
67. Miller, J.D.; Knapp, E.E.; Key, C.H.; Skinner, C.N.; Isbell, C.J.; Creasy, R.M.; Sherlock, J.W. Calibration and validation of the relative differenced normalized burn ratio (RDNBR) to three measures of fire severity in the Sierra Nevada and Klamath mountains, California, USA. *Remote Sens. Environ.* **2009**, *113*, 645–656. [CrossRef]
68. Moran, P.A.P. Notes on continuous stochastic phenomena. *Biometrika* **1950**, *37*, 17–23. [CrossRef] [PubMed]
69. Li, H.; Calder, C.A.; Cressie, N. Beyond Moran's I: Testing for spatial dependence based on the spatial autoregressive model. *Geogr. Anal.* **2007**, *39*, 357–375. [CrossRef]

70. Westerling, A.; Turner, M.; Smithwick, E.; Romme, W.; Ryan, M. Continued warming could transform greater Yellowstone fire regimes by mid-21st century. *Proc. Natl. Acad. Sci. USA* **2011**, *108*, 13165–13170. [CrossRef] [PubMed]
71. Turner, M.G.; Romme, W.H.; Tinker, D.B. Surprises and lessons from the 1988 Yellowstone fires. *Front. Ecol. Environ.* **2003**, *1*, 351–358. [CrossRef]
72. Attiwill, P.M. The disturbance of forest ecosystems: The ecological basis for conservative management. *For. Ecol. Manag.* **1994**, *63*, 247–300. [CrossRef]
73. Dolan, K.; Masek, J.G.; Huang, C.; Sun, G. Regional forest growth rates measured by combining ICESat GLAS and Landsat data. *J. Geophys. Res. Biogeosci.* **2009**, *114*, 1–7. [CrossRef]
74. Helmer, E.H.; Lefsky, M.A.; Roberts, D.A. Biomass accumulation rates of amazonian secondary forest and biomass of old-growth forests from Landsat time series and the geoscience laser altimeter system. *J. Appl. Remote Sens.* **2009**, *3*, 033505.
75. Helmer, E.H.; Ruzycki, T.S.; Wunderle, J.M.; Vogesser, S.; Ruefenacht, B.; Kwit, C.; Ewert, D.N. Mapping tropical dry forest height, foliage height profiles and disturbance type and age with a time series of cloud-cleared Landsat and ali image mosaics to characterize avian habitat. *Remote Sens. Environ.* **2010**, *114*, 2457–2473. [CrossRef]
76. Frazier, R.J.; Coops, N.C.; Wulder, M.A. Boreal shield forest disturbance and recovery trends using Landsat time series. *Remote Sens. Environ.* **2015**, *170*, 317–327. [CrossRef]
77. Pickell, P.D.; Hermosilla, T.; Frazier, R.J.; Coops, N.C.; Wulder, M.A. Forest recovery trends derived from Landsat time series for North American boreal forests. *Int. J. Remote Sens.* **2016**, *37*, 138–149. [CrossRef]
78. Wijdeven, S.M.; Kuzee, M.E. Seed availability as a limiting factor in forest recovery processes in Costa Rica. *Restor. Ecol.* **2000**, *8*, 414–424. [CrossRef]
79. Savage, M.; Brown, P.M.; Feddema, J. The role of climate in a pine forest regeneration pulse in the southwestern United States. *Ecoscience* **1996**, *3*, 310–318. [CrossRef]
80. Simpson, R.; Leck, M.A.; Parker, V. Seed banks: General concepts and methodological issues. *Ecol. Soil Seed Banks* **1989**, *1*, 3–8.
81. Frank, D.A.; McNaughton, S.J. The ecology of plants, large mammalian herbivores, and drought in Yellowstone National Park. *Ecology* **1992**, *73*, 2043–2058. [CrossRef]
82. Li, A.; Huang, C.; Sun, G.; Shi, H.; Toney, C.; Zhu, Z.; Rollins, M.G.; Goward, S.N.; Masek, J.G. Modeling the height of young forests regenerating from recent disturbances in Mississippi using Landsat and ICESat data. *Remote Sens. Environ.* **2011**, *115*, 1837–1849. [CrossRef]
83. Romme, W.H.; Knight, D.H. Fire frequency and subalpine forest succession along a topographic gradient in Wyoming. *Ecology* **1981**, *62*, 319–326. [CrossRef]
84. Turner, M.G.; Romme, W.H.; Gardner, R.H. Prefire heterogeneity, fire severity, and early postfire plant reestablishment in subalpine forests of Yellowstone National Park, Wyoming. *Int. J. Wildland Fire* **1999**, *9*, 21–36. [CrossRef]
85. Turner, M.G.; Baker, W.L.; Peterson, C.J.; Peet, R.K. Factors influencing succession: Lessons from large, infrequent natural disturbances. *Ecosystems* **1998**, *1*, 511–523. [CrossRef]